

Classical and non-classical time history and spectrum analysis of soil-structure interaction systems

F. Behnamfar¹ · H. Alibabaei¹

Received: 10 January 2016 / Accepted: 16 August 2016 / Published online: 6 September 2016
© Springer Science+Business Media Dordrecht 2016

Abstract The problem of non-classical dynamic analysis of structures resting on flexible bases is studied in this paper. Because of presence of the underlying soil in the dynamic model of structure that acts like an energy sink, the damping matrix is not proportional to structural mass and stiffness and theoretically a non-classical approach should be followed in modal analysis. Considering one to twenty-story buildings, two types of soils, and several suits of ground motions each containing ten earthquake records specifically selected for each building, the seismic responses are calculated using a time history modal analysis in this paper. Three cases are considered: fixed-base buildings with classical analysis, flexible-base buildings with classical and non-classical analysis. It is shown that the code-based soil-structure interaction (SSI) analysis for the fundamental mode is not always safe. Also, on each soil type, instances of importance of accounting for the non-classical nature of the SSI system are clarified. Cases for which the base flexibility should be considered for the higher modes too are distinguished. Finally, simple correction factors are derived for converting the fixed-base responses of moment frames, resting on surface foundations on medium and soft soils, to the responses including soil-structure interaction effects.

Keywords Nonclassical · Time history · Spectrum · Soil-structure interaction

1 Introduction

Modeling of the soil-structure interaction (SSI) is meant to be a more accurate and realistic approach to a structural analysis problem; then, a more detailed modeling of the damping phenomenon in the system is warranted in this case. This task is performed by putting aside

✉ F. Behnamfar
farhad@cc.iut.ac.ir

¹ Department of Civil Engineering, Isfahan University of Technology, Esfahan 8415683111, Iran

the convenient assumption that damping is proportional to mass and stiffness, i.e., by doing a nonclassical dynamic analysis. In an SSI system a considerable part of damping, called the radiation damping, is contributed by the totally different medium of soil by letting the structural vibration energy propagate toward infinity from the soil-structure interface, or the foundation. This is unlike the fixed-base systems in which the source of vibration damping is more or less uniquely attributed to the structural system and is hence almost uniform. Therefore, when the flexibility of soil is accounted for in the seismic analysis of structures resting on such a medium, the system damping matrix is no longer taken to be proportional to structure's mass and stiffness matrices. The damping matrix of such a complex system is a non-uniform combination of structure and soil damping values and therefore is not classical.

On the other hand, when only the maxima of seismic responses are sought (which is the prevailing case), the spectrum analysis can help attain a relatively rapid yet accurate enough design in most problems. A basic assumption in such an analysis is the damping being classical. This makes definition of the damping matrix very easily possible as a combination of mass and stiffness matrices. When there is a doubt on validity of this basic assumption, like in SSI problems as discussed above, availability of a spectrum analysis methodology corrected for nonclassical damping while retaining its simplicity will be very helpful.

Many attempts have been made by different researchers to develop dynamic analysis methods for systems with a nonclassical damping. The first solution for dynamic response of such systems was derived by Foss (1958). His method is known as the extended modal analysis (EMA). While being robust, the complexity of the above method detracted the attention of practical engineers. The work of Veletsos and Ventura (1986) was an important step forward in this regard. They simplified the EMA through giving insight to the physical meaning of different terms of the formulation and converted the complex-valued equations to their real counterparts. They derived equations for determining natural periods and mode shapes of nonclassical systems resulting in free vibration responses and a Duhamel integral formulation for computing the dynamic response.

The response spectrum analysis consists of two steps: computing the maxima in each mode, and, combining the modal maximum responses via a suitable rule like SRSS or CQC. Ziaiefar and Tavousi (2005) developed formulas for calculating the modal values of the response maxima based on the work of Veletsos and Ventura (1986). They applied their formulation to mass-isolated structural systems and studied the conditions requiring such nonclassical analysis. Zhou and Yu (2008) derived formulas for combining the maximum modal responses of non-classically damped linear systems. They used the random vibration theory and accounted for the correlation between the modal displacement and velocity responses of structure. Based on a general modal response history analysis formulation for nonclassical and over-damped systems developed by Song et al. (2008), they derived a response spectrum analysis approach and proposed a general modal combination rule.

To gain attractiveness in practical earthquake engineering, a nonclassical SSI problem should be solved within the frame work of a conventional design spectrum. In the code-based procedures (American Society of Civil Engineers 2010), it is prescribed that for spectral analysis of SSI systems, the fixed-base design spectrum of the code is still used but with the fundamental period and equivalent damping of the SSI system, which are usually larger than those of the fixed-base system. This prescribed analysis is only for the fundamental mode and the effect of SSI on the higher modes is allowed to be ignored.

In the current study, first the SSI base shear and displacements are compared with their fixed-base counterparts using both classical and nonclassical analysis. Then, it is recognized for which cases the higher mode SSI effects are important and in what instances performing the non-classical SSI analysis is necessary. One to 20-story buildings are considered and for each building, two suits of ground motion each containing 10 records, one being recorded at the near field and the other at the far field, selected through a special procedure specifically for each structure are used. Two types of medium and soft soils are also considered.

In the following, first the theory of non-classical spectral analysis of SSI systems is described and then the building-earthquakes cases are identified and the analysis results are presented.

2 Modal analysis of soil-structure systems

In this section the equations of motion of structures resting on flexible soils are derived and decomposed into its modal components as an extension of (Veletsos and Ventura 1986) to soil-structure systems. To this end, a multistory structure on flexible soil subjected to a horizontal ground motion is considered as shown in Fig. 1.

Without curbing generality, the system is assumed to be a shear building having a single horizontal degree of freedom (DOF) at each floor to retain simplicity. In addition, it is supposed that the supporting medium possesses a horizontal as well as a rotational DOF, and the input motion in the presence of structure is assumed to be identical to the free-field motion.

The equations of motion of the system of Fig. 1 can be written as follows:

$$[M]\{\ddot{U}\} + [C]\{\dot{U}\} + [K]\{U\} = p(t) \tag{1}$$

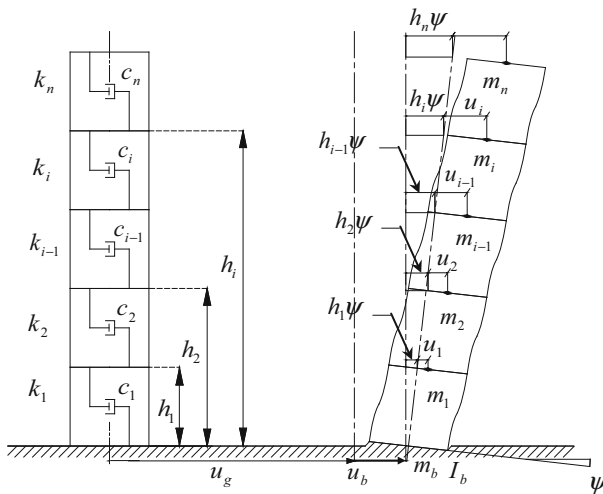


Fig. 1 The multistory structure on flexible soil under lateral movement

in which:

$$\{U\} = \begin{Bmatrix} \{u\} \\ u_b \\ \psi \end{Bmatrix} \tag{2}$$

$$\{p(t)\} = - \left\{ \{m\} \quad m_b + \sum_1^n m_i \quad \sum_1^n m_i h_i \right\}^T \ddot{u}_g(t) \tag{3}$$

and the mass, damping and stiffness matrices are shown with $[M]$, $[C]$ and $[K]$, respectively, introduced in Eqs. (24–28) in the Appendix. As seen with the vector of degrees of freedom in Eq. (2), the additional two last rows refer to the extra deformations at the base. This in turn results in the fact that the two last rows and columns of the damping matrix pertain to the soil dampings. This property makes the total system damping matrix to be in essence nonclassical, i.e., non-proportional to mass and stiffness matrices. Of course, it can be assumed to be proportional just as an approximate presumption.

As shown in Appendices 2 and 3, the dynamic response including non-proportionality of the damping matrix can be derived as:

$$\{U\} = \sum_{j=1}^N \left[\{ \alpha_j^v \} V_j(t) + \{ \beta_j^v \} \dot{D}_j(t) \right] \tag{4}$$

in which $V_j(t)$ and $\dot{D}_j(t)$ are the pseudo-velocity and the relative velocity of the j th mode equivalent SDF system with natural frequency p_j and damping ratio ζ_j (see Eq. 33), N is the total number of degrees of freedom, and $\{ \alpha_j^v \}$ and $\{ \beta_j^v \}$ are as defined in Eqs. (50) and (45), respectively. $V_j(t)$ and $\dot{D}_j(t)$ are defined as follows:

$$V_j(t) = p_j D_j(t) = -p_j \int_0^t \ddot{u}_g(\tau) h_j(t - \tau) d\tau \tag{5}$$

$$\dot{D}_j(t) = - \int_0^t \ddot{u}_g(\tau) \dot{h}_j(t - \tau) d\tau$$

The base shear is computed as described in Appendix 4 as the summation of lateral story forces resulting in the following equation:

$$V^b(t) = \sum_{j=1}^N \left[\left(m_j^{\omega} \right) p_j V_j(t) + \left(m_j^{\beta\gamma} \right) p_j \dot{D}_j(t) \right] \tag{6}$$

in which:

$$\begin{aligned} m_j^{\omega} &= \alpha_j^{Mv} + \omega_j^{Mv} \\ m_j^{\beta\gamma} &= \beta_j^{Mv} + \gamma_j^{Mv} \end{aligned} \tag{7}$$

and $\langle 1_N \rangle = \left\langle \overbrace{1 \dots 1}^n \quad 0 \quad 0_{n+2} \right\rangle$, and the quantities on the right side of Eq. (7) are as defined in Eq. (58).

3 The spectrum analysis

In order to calculate the maximum displacements or base shear from Eqs. (4) or (6), respectively, maximum values of $V_j(t)$ and $\dot{D}_j(t)$ are needed noting that these maxima need not to occur simultaneously. One may use the SRSS rule to combine these maxima as:

$$\begin{aligned} \{U\}_{j_{\max}} &= \sqrt{\left(\{\alpha_j^v\}V_{j_{\max}}\right)^2 + \left(\{\beta_j^v\}\dot{D}_{j_{\max}}\right)^2} \\ V_{j_{\max}}^b &= \sqrt{\left(\left(m_j^{\alpha\omega}\right)p_jV_{j_{\max}}\right)^2 + \left(\left(m_j^{\beta\gamma}\right)p_j\dot{D}_{j_{\max}}\right)^2} \end{aligned} \tag{8}$$

in which, an index max shows the maximum value in the j th mode. The following relation can be assumed to exist between the maximum values of $V_j(t)$ and $\dot{D}_j(t)$:

$$\dot{D}_{j_{\max}} = \eta_j V_{j_{\max}} \tag{9}$$

There have been different proposals for the conversion factor η_j in the above equation. Sinha and Igusa (1995) used an $\eta_j = 1$ assumption. Zhou and Yu (2008) used the theory of random vibrations to calculate the correlation factors of displacement and velocity functions in each mode. Sadek et al. (2000) proposed the following relation using the period T_j and damping factor ξ_j of the j -th mode:

$$\begin{aligned} \eta_j &= a_{vj}T_j^{b_{vj}}, \quad a_{vj} = 1.095 + 0.647\xi_j - 0.382\xi_j^2 \\ b_{vj} &= 0.193 + 0.838\xi_j - 0.621\xi_j^2 \end{aligned} \tag{10}$$

Ziaiefar and Tavousi (2005) based on a work by Pekcan et al. (1999) suggested that:

$$\eta_j = f(T_j, \xi_j) = 0.8 - 0.6\xi_j + 0.17T_j + 0.4\xi_j T_j \tag{11}$$

The above equation is on the basis of the random vibration analysis of an earthquake ground motion assumed to be a stationary function, and is used in this study.

Substituting (9) in (8) results in:

$$\begin{aligned} \{U\}_{j_{\max}} &= \sqrt{\{\alpha_j^v\}^2 + \eta_j^2 \{\beta_j^v\}^2} V_{j_{\max}} \\ V_{j_{\max}}^b &= \sqrt{\left(m_j^{\alpha\omega}\right)^2 + \eta_j^2 \left(m_j^{\beta\gamma}\right)^2} p_j V_{j_{\max}} \end{aligned} \tag{12}$$

Equation (12) can be simplified to give the maximum base shear of the j th mode as:

$$V_{j_{\max}}^b = M_j p_j S_{pv}(p_j, \xi_j) = M_j S_{pa}(p_j, \xi_j) \tag{13}$$

in which:

$$M_j = \sqrt{\left(m_j^{\alpha\omega}\right)^2 + \eta_j^2 \left(m_j^{\beta\gamma}\right)^2} \tag{14}$$

where S_{pv} and S_{pa} are the spectral values of the j th mode pseudo-velocity and pseudo-acceleration, respectively.

Equation (13) for computing the maximum base shear of a nonclassical SSI system differs from that of the classical (conventional) systems in two ways. First, the pseudo-acceleration S_{pa} should be calculated using the j th mode period and damping ratio of the nonclassical system, and second, a different modal mass M_j calculated by Eq. (14) is utilized.

4 Numerical modeling

4.1 Design assumptions

For the purposes of this study, special steel moment frame structures being 1, 2, 4, 6, ..., 18 and 20 story building are designed. The frames have three bays both ways each spanning 5 m. The floor to floor heights are 3 m. The residential buildings are designed according to ASCE 7-10 (American Society of Civil Engineers 2010) and AISC-ASD (American Institute of Steel Construction 2005). The seismicity of the region is considered to be very high with the effective peak acceleration at the ground surface to be 0.35 g. Two types of underlying soils are considered: a soft soil [soil type D (American Society of Civil Engineers 2010)] and a very soft soil (soil type E). Their characteristics are given in Table 1.

Eleven buildings with the mentioned number of stories are designed with fixed bases for each soils type. Therefore, totally 22 buildings are considered in this study. The design spectra are shown in Fig. 2 for each soil type (American Society of Civil Engineers 2010).

Natural periods of the buildings in their first three modes of lateral displacement are shown in Table 2.

As seen in Table 2, since the same building is designed using a different spectrum on each soil type, two different buildings with the same height but different periods are resulted. For 1 to 4-story buildings single footings and for 6 to 20-story structures strip foundations are designed. The foundation dimensions are shown in Table 3.

4.2 The earthquake records

After design of fixed-base buildings, they will be analyzed under seismic ground motions for calculating their dynamic responses. For time-history analysis of the buildings under study, earthquake records with the following characteristics are selected out of the PEER NGA database (http://peer.berkeley.edu/peer_ground_motion_database): $6.5 \leq \text{Magnitude} \leq 7.5$, soil type is whether D or E. Two groups of earthquakes are selected for each building on each soil type regarding the epicentral distance, R . Group one, the near-field earthquakes with $R \leq 20$ km, and group two, the far-field earthquakes with

Table 1 Characteristics of the soil types

Soil type	Shear wave velocity V_s (m/s)	Unit mass ρ (kg/m ³)	Poisson's ratio ν	Bearing capacity (kgf/cm ²)
D	250	1800	0.4	2
E	125	1700	0.45	1.5

Fig. 2 The design spectra for the soil types D and E

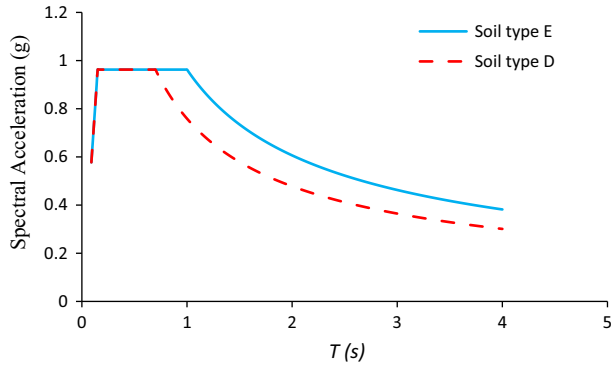


Table 2 First three natural periods of the fixed-base buildings in lateral motion (s)

Soil type	Type D			Type E		
	Mode 1	Mode 2	Mode 3	Mode 1	Mode 2	Mode 3
No. of stories						
1	0.555	–	–	0.555	–	–
2	0.768	0.315	–	0.768	0.315	–
4	0.971	0.399	0.257	0.971	0.399	0.257
6	1.19	0.490	0.313	1.19	0.490	0.313
8	1.42	0.567	0.352	1.36	0.548	0.347
10	1.72	0.699	0.438	1.52	0.603	0.385
12	1.93	0.770	0.481	1.74	0.688	0.428
14	2.06	0.840	0.529	1.94	0.777	0.485
16	2.34	0.939	0.578	2.12	0.828	0.515
18	2.56	1.02	0.627	2.35	0.980	0.620
20	2.81	1.10	0.682	2.49	0.972	0.600

20 < R ≤ 50 km. Then the records are scaled according to ASCE7-10 (American Society of Civil Engineers 2010), such that their response spectra does not fall below the design spectrum of Fig. 2 between 0.2T and 1.5T, where T is the fundamental period of the fixed-base buildings. Then 10 records in each distance group with scale factors closer to unity (hence with more similarity to the design spectrum) are retained for dynamic analysis of the same building. Table 4 shows the records selected for each building. Also, for instance, Table 5 shows the records selected for the 10-story building along with their scale factors. Characteristics of the selected records of Table 4 are given in the Appendix.

4.3 Modeling of soil-structure interaction

For the purposes of this study it is necessary to analyze four different models. Model 1 and Model 2 are two-dimensional (2D) frames representing an interior frame of each of the above buildings developed in SAP2000 (Computers and Structures, Inc. 2014). Model 1 is

Table 3 Dimensions of the foundations (m)

Number of stories	Foundation type	Soil type D	Soil type E
1	Footing	Exterior: $0.9 \times 0.9 \times 0.5$ Interior: $1.1 \times 1.1 \times 0.5$	Exterior: $1 \times 1 \times 0.5$ Interior: $1.1 \times 1.1 \times 0.5$
2	Footing	Exterior: $1.1 \times 1.1 \times 0.5$ Interior: $1.3 \times 1.3 \times 0.5$	Exterior: $1.2 \times 1.2 \times 0.6$ Interior: $1.5 \times 1.5 \times 0.6$
4	Footing	Exterior: $1.3 \times 1.3 \times 1$ Interior: $1.8 \times 1.8 \times 1$	Exterior: $1.7 \times 1.7 \times 1$ Interior: $2.1 \times 2.1 \times 1$
6	Strip	$15.5 \times 1 \times 0.7$	$15.5 \times 1.4 \times 1$
8	Strip	$15.5 \times 1.4 \times 0.7$	$15.5 \times 1.7 \times 1$
10	Strip	$15.5 \times 1.7 \times 1$	$16 \times 2.3 \times 1$
12	Strip	$15.5 \times 2.1 \times 1$	$16.5 \times 2.7 \times 1$
14	Strip	$16 \times 2.5 \times 1$	$17 \times 2.8 \times 1$
16	Strip	$16.5 \times 2.6 \times 1.2$	$18 \times 3 \times 1.2$
18	Strip	$17 \times 2.8 \times 1.2$	$18.5 \times 3.2 \times 1.2$
20	Strip	$17 \times 3.1 \times 1.2$	$19 \times 3.5 \times 1.2$

Table 4 The selected records

Soil type D				Soil type E			
Near field		Far field		Near field		Far field	
NGA number	PGA (g)	NGA number	PGA (g)	NGA number	PGA (g)	NGA number	PGA (g)
953	0.55	169	0.28	178	0.26	726	0.13
1044	0.70	777	0.23	1038	0.15	732	0.08
1063	0.63	778	0.26	1111	0.49	1107	0.27
1085	0.65	786	0.21	1113	0.08	1180	0.13
1087	0.99	806	0.21	1116	0.23	1183	0.12
1197	0.79	987	0.25	1119	0.71	1196	0.06
1492	0.35	995	0.37	1120	0.65	1199	0.09
1503	0.66	996	0.34	1194	0.15	1204	0.11
1504	0.41	1001	0.27	1496	0.14	1205	0.46
1507	0.62	1003	0.45	1536	0.18	1228	0.08
1508	0.40	1186	0.24	1541	0.17	1233	0.07
1509	0.45	1187	0.16	–	–	1238	0.10
1529	0.24	1201	0.30	–	–	1240	0.06
1602	0.77	1203	0.26	–	–	1246	0.18
1605	0.43	1236	0.18	–	–	1483	0.13
–	–	1478	0.18	–	–	1537	0.11
–	–	1484	0.21	–	–	1538	0.08
–	–	–	–	–	–	1542	0.13
–	–	–	–	–	–	1553	0.09

Table 5 The selected records and their scale factors for the 10 story building

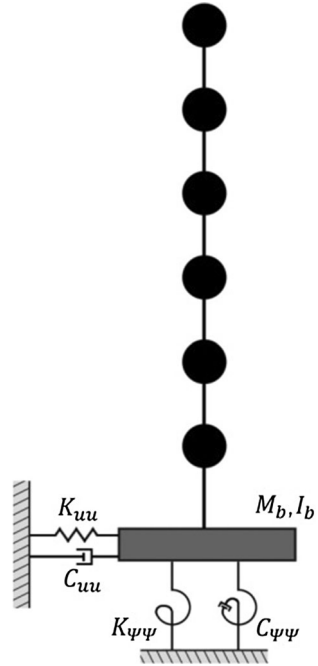
Soil type D				Soil type E			
Near field		Far field		Near field		Far field	
NGA number	Scale factor	NGA number	Scale factor	NGA number	Scale factor	NGA number	Scale factor
953	0.4759	169	0.7058	178	1.3794	732	0.870
1044	0.473	777	0.612	1111	0.582	1107	1.104
1087	0.577	778	0.880	1113	2.353	1180	1.265
1197	0.501	806	1.226	1116	1.239	1199	1.548
1504	0.406	1187	0.923	1119	0.409	1204	1.402
1507	0.698	1201	0.645	1120	0.255	1238	1.348
1508	0.602	1203	0.729	1194	1.030	1246	1.085
1529	0.435	1236	0.832	1496	1.360	1537	1.324
1602	0.791	1478	1.178	1536	0.609	1542	0.802
1605	0.614	1484	1.211	1541	0.992	1553	1.317

fixed at base but Model 2 is a flexible base structure. Flexibility of the base in Model 2 is incorporated by adding the body of foundations to the structural model while resting on certain springs. Calculation of the stiffness of the soil springs is described in the next section.

Moreover, an equivalent damping accounting for combination of the dampings of the structure and the soil is determined, as explained in Sect. 4.3.2, and assigned to the flexible-base model. The structural part of the damping is assumed to be of Rayleigh type with a damping ratio of 5 % in all models. Models 3 and 4 are stick models of the same flexible-base 2D frames as above and are developed in Matlab. Models 1–3 are analyzed using the classical modal analysis and Model 4 using the nonclassical procedure described in Sects. 2 and 3. The reason for Model 3 is utilizing it as a basis for comparison, within the needs of this study, with responses determined using the more accurate 2D frame analysis (Model 2) in SAP. This is needed because certain simplifying assumptions are necessary to reduce a 2D model to a stick model. Model 4 is necessary for nonclassical analysis because such an analysis is not possible in commercial engineering softwares. In both models 3 and 4, the flexible base is modeled using a rigid foundation being in dimensions equivalent to the actual foundations of the 2D frames. For strip foundations (in 6 to 20-story buildings), the same dimensions are used. For single footings (in 1 to 4-story buildings), length of the foundation element in Models 3 and 4 is taken to be equal to sum of the single foundation lengths in the corresponding 2D frames. Width of the foundation in this case is mean of the foundation widths in the corresponding frame. The above assumptions are easily validated by doing the same seismic analysis for the Models 2 and 3. It will be shown that the mentioned assumptions are appropriate for the responses targeted in this study.

The base of the Models 3 and 4 rests on springs and dampers along the two degrees of freedom in plane as shown in Fig. 3. Characteristics of the springs and dampers are given in the following sections.

Fig. 3 Configuration of the stick models (Models 3 and 4)



4.3.1 Stiffness of the soil springs

The stiffness of soil springs is a function of the dynamic shear modulus of soil, G . The dynamic shear modulus can be much smaller than the soil shear modulus at small strains, G_0 , because of the large strains that develop in soil during an earthquake. G_0 is given by Eq. (15):

$$G_0 = \frac{\gamma V_s^2}{g} = \rho V_s^2 \tag{15}$$

in which γ is the unit weight of soil, V_s is the shear wave velocity in soil at small strains, and g is the acceleration of gravity. The ratio G/G_0 depends on the soil type and the soil’s shear strain during earthquake. Since the shear strain is somewhat correlated with the peak ground acceleration and the latter with the spectral acceleration, the ratio G/G_0 has appeared in the codes as a function also of the effective peak ground acceleration at the ground surface (S_{DS}) for simplicity. S_{DS} is equal to the spectral acceleration at short periods divided by 2.5 (American Society of Civil Engineers 2010). Values of G/G_0 for the two soil types are given in Table 6 according to ASCE 7-10 (American Society of Civil Engineers 2010).

Since different ground motions have been selected for different structures, the average S_{DS} of each group of earthquakes mentioned in Table 4 is used for calculation of G/G_0 on each soil type.

According to ASCE41-13 (American Society of Civil Engineers 2013), before determining the spring stiffnesses, condition of the foundation being flexible or rigid with regard to the underlying soil, must be determined. Then, if the inequalities (16) and (17) hold, the single/mat and strip foundations, respectively, are rigid:

Table 6 Values of G/G_0

Soil type	Type D		Type E	
	Near field	Far field	Near field	Far field
No. of stories				
1	0.393	0.682	0.210	0.357
2	0.389	0.726	0.225	0.375
4	0.408	0.679	0.225	0.458
6	0.258	0.703	0.225	0.531
8	0.353	0.708	0.225	0.538
10	0.252	0.721	0.225	0.472
12	0.277	0.738	0.225	0.552
14	0.376	0.738	0.225	0.552
16	0.264	0.715	0.225	0.567
18	0.339	0.711	0.225	0.558
20	0.250	0.732	0.225	0.558

$$4k_{sv} \sum_{m=1}^5 \sum_{n=1}^5 \frac{\sin^2 \left[\frac{m\pi}{2} \right] \sin^2 \left[\frac{n\pi}{2} \right]}{\pi^4 D_f \left[\frac{m^2}{L^2} + \frac{n^2}{B^2} \right]^2 k_{sv}} < 0.3 \tag{16}$$

$$D_f = \frac{E_f t^3}{12(1 - \nu_f)^2}, \quad k_{sv} = \frac{1.3G}{B(1 - \nu)}$$

$$\frac{E_f I_f}{l^4} > \frac{2}{3} k_{sv} B \tag{17}$$

where E_f and ν_f are respectively the modulus of elasticity and the Poisson’s ratio of foundation material (concrete); B , L and t are width, length, and thickness of foundation, ν and G are the Poisson’s ratio and (dynamic) shear modulus of soil, k_{sv} is the vertical stiffness of soil (or the modulus of soil reaction) and I_f and l are moment of inertia of the strip foundation’s section and its length shared by one column, respectively.

The above criteria result in all of the foundations of this study resting on the soil type E to be rigid. For the soil type D, only foundations of 1, 2 and 4-story buildings prove to be rigid. This is expected because of the small dimensions of the footings for the shorter buildings and softness of the soil types. In the plane of a 2D frame, introducing the horizontal x and the vertical z translational and the y -axis rocking degrees of freedom at each foundation component suffice. Following the linear procedure of ASCE41-13 (American Society of Civil Engineers 2013), for each foundation, a single horizontal spring is assigned in the x direction. For flexible foundations, a uniformly distributed vertical spring with the stiffness k_{sv} given in Eq. (16) is utilized.

For rigid foundations, coupling of vertical and rocking degrees of freedom is taken into account using a nonuniform distribution of vertical springs. For this purpose, each foundation is divided to interior and exterior zones. The exterior zones are two rectangles, one at each end of the foundation, with a length of $B/6$ and a width equal to that of the foundation.

The vertical stiffness of the distributed springs at the middle and end zones, k_{mid} and k_{end} respectively, are as follows (American Society of Civil Engineers 2013):

$$k_{end} = \frac{6.83G}{1 - \nu} \quad (18)$$

$$k_{mid} = \frac{0.73G}{1 - \nu}$$

The distance between the vertical springs is taken to be about 20 cm on average.

4.3.2 Damping

As mentioned at the beginning of Sect. 4.3, an equivalent damping ratio accounting for the effects of base flexibility is used with Model 2. It is calculated using Eq. (19) (American Society of Civil Engineers 2010):

$$\bar{\beta} = \beta_0 + \frac{\beta}{\left(\frac{\bar{T}}{T}\right)^3} \quad (19)$$

in which $\bar{\beta}$ is the equivalent SSI damping ratio of structure, β_0 is the damping ratio supplied by foundation and soil as being a function of \bar{T}/T and aspect ratio of structure (American Society of Civil Engineers 2010), β is the damping ratio of the fixed-base structure (assumed to be equal to 0.05), \bar{T} is the fundamental period of structure including SSI, and T is the fundamental period of the fixed-base building. Use of Eq. (19) results in $\bar{\beta}$ values to be as listed in Table 7. According to Sect. 4.3.1, stiffness properties of soil and therefore values of \bar{T} are functions of G , itself being a function of S_{DS} as of Table 6 and its descriptions. Therefore, $\bar{\beta}$ values are different when analyzing the 2D frames of this study under near and far field earthquakes. Values of \bar{T}/T are given in Sect. 5.2.

Design spectra as shown in Fig. 2 are given for a damping ratio of 0.05, as common. For SSI applications, the spectral values will be needed for other damping ratios, as given in Table 7, too. This is usually done using a spectral reduction factor RF . Many versions are

Table 7 Values of the equivalent damping ratios of structures including SSI, $\bar{\beta}$

Soil type	Type D		Type E	
	Near field (%)	Far field (%)	Near field (%)	Far field (%)
No. of stories				
1	9.8	10	8.7	9.2
2	10.4	10.5	10.1	10.5
4	11.3	11.4	11.6	11.7
6	11.9	12.1	12.1	12.6
8	12.6	12.7	12	12.7
10	12.8	13	12.6	13.3
12	13.1	13.4	12.7	13.7
14	13.7	13.9	13	13.9
16	13.5	14	13.2	14.1
18	14	14.3	13.4	14.4
20	14	14.6	13.6	14.6

available for RF as proposed by different researchers, such as those of Newmark and Hall (1982), Ashour (1987), Wu and Hanson (1989), Ramirez et al. (2002), Lin and Chang (2003) and Bommer and Mendis (2005). The equation given by Bommer and Mendis has been endorsed by several building codes like Eurocode 8 (2003) and is used in this study for spectrum modification. It is given in Eq. (20):

$$RF = \begin{cases} 1 - (1 - \eta) \frac{\bar{T}}{T_b} & 0 \leq \bar{T} < T_b \\ \eta & \bar{T} \geq T_b \end{cases}, \quad \eta = \sqrt{\frac{10}{5 + 100\beta}} \geq 0.55 \quad (20)$$

in which T_b is the period at which the constant acceleration branch begins in the Newmark spectrum, being equal to $\frac{1}{8}$ s. According to Fig. 3, for Models 3 and 4 explicit representation of dampers has been adopted. The damping coefficients in the horizontal and rocking degrees of freedom have been given as (Gazetas 1991):

$$C_{uu} = pV_s A_b \quad (21)$$

$$C_{\psi\psi} = pV_{la} I_{by} \tilde{c}_{ry}$$

where p is the unit mass of soil, A_b is the area of foundation in plan, I_{by} is the moment of inertia of the foundation in plan about the transverse axis, V_{la} is a wave velocity equal to $\frac{3.4V_s}{\pi(1-\nu)}$ with V_s being the shear wave velocity, and \tilde{c}_{ry} is a coefficient beginning from zero for the static case and tending to unity for very large excitation frequencies.

5 The analysis results

In this section, after a comparison between the analytical models, first the natural periods and damping ratios are calculated for the SSI systems. Then, the maxima of base shear and lateral displacement of roof of each building are determined for the all four models of Sect. 4.3. For this purpose, a linear dynamic time history analysis is utilized and the results of each response parameter are averaged between the earthquakes corresponding to each building. Then the responses are shown against the fixed-base natural period.

5.1 Comparison of the flexible-base 2D and stick models responses

As mentioned in Sect. 4.3, two different models, called Models 2 and 3, are used for representing the seismic responses of the flexible base systems, using the classical procedure. Model 2 is a planar frame in SAP including beams, columns, and the single footing of each column or the whole strip footing resting on the vertical springs described in Sect. 4.3.1. Model 3 is a stick model displayed in Fig. 3 with stiffness and damping properties described in Sects. 4.3.1 and 4.3.2. Since the same stick model will be used for the nonclassical analysis procedure too (Model 4, because nonclassical analysis is not possible in SAP), Model 3 is meant to act as a basis of comparison for Model 4. Therefore, Model 3 needs to be justified first with a more accurate system like Model 2.

Figure 4 shows values of the base shear calculated using Model 2 in SAP and Model 3 in Matlab, normalized to the weight of each building. The results are presented separately for the near-field and far-field earthquakes and for different soil types. Average of the maximum response in linear time history analysis of each building is shown for each building on each soil type under near and far field earthquakes by finding its fixed-base

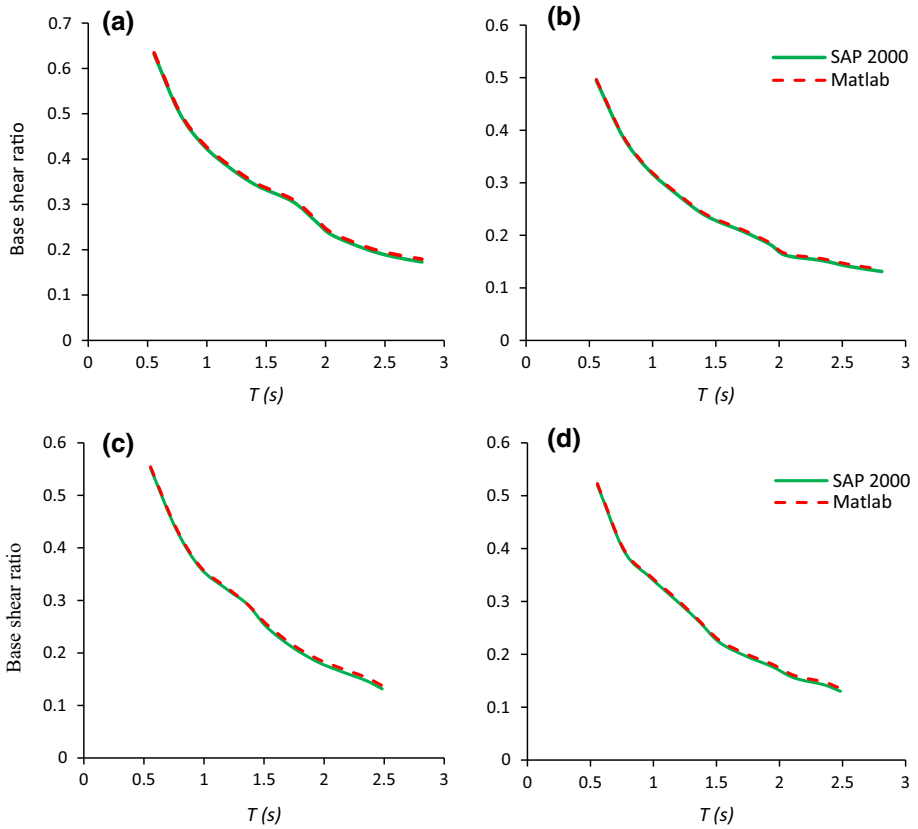


Fig. 4 Values of the base shear for the classical flexible-base 2D and stick models normalized to the building weight, versus the fixed-base period T . **a** Soil type D, near field earthquakes. **b** Soil type D, far field earthquakes. **c** Soil type E, near field earthquakes. **d** Soil type E, far field earthquakes

natural period on the horizontal axis. Similarly, values of the maximum lateral displacement normalized to the height of each building are shown in Fig. 5.

As observed, the base shear values calculated by Models 2 and 3 are practically the same. For the maximum roof displacement again a very good similarity is observed, with the relative difference being larger for the taller buildings and reaching a value of about 6 % for the tallest frame. Along the period axis, the displacements are always overestimated by the stick model. Therefore, Model 4 is an appropriate model for nonclassical analysis and Model 3, being almost equivalent to Model 2 and having a similar configuration to Model 4, is a suitable reference for comparison with Model 4.

5.2 The natural periods and damping ratios

Figure 6 shows the values of the first to the third natural periods of the flexible-base systems normalized to the corresponding values of the same systems but fixed at base. The latter values are given in Table 2. Periods of the flexible-base systems have been calculated using Models 3 and 4. Therefore, in each part of the figure results of analysis of classical and nonclassical systems are given together for ease of comparison. Because system

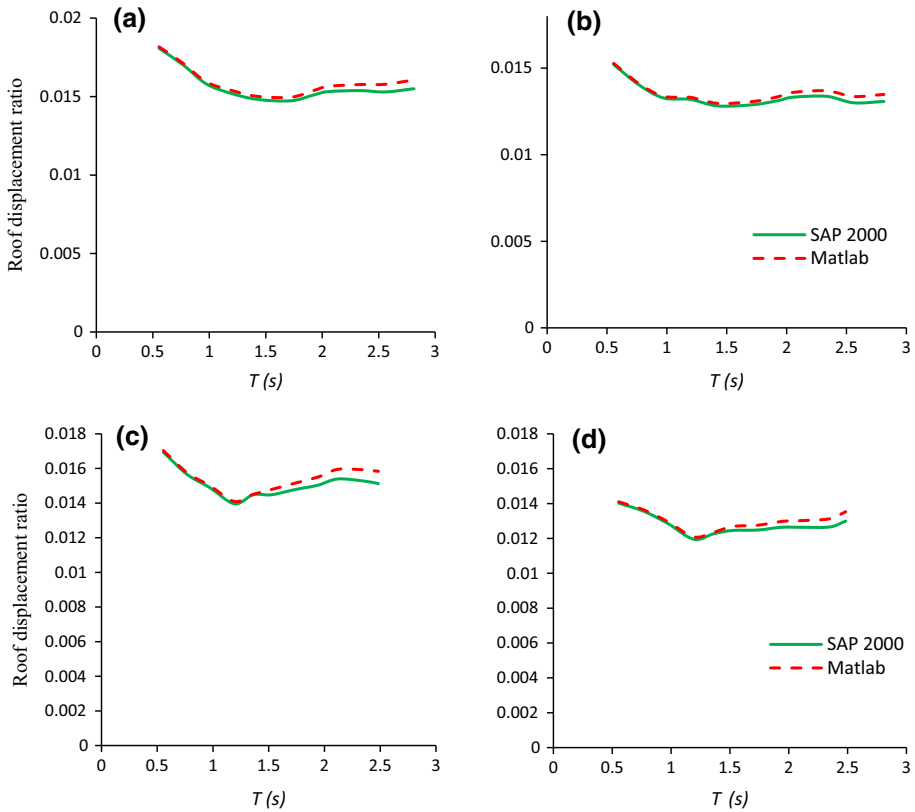


Fig. 5 Values of the maximum roof displacement for the classical flexible-base 2D and stick models normalized to the building height, versus the fixed-base period T . **a** Soil type D, near field earthquakes. **b** Soil type D, far field earthquakes. **c** Soil type E, near field earthquakes. **d** Soil type E, far field earthquakes

stiffness changes also with G/G_0 (Table 5), values are averaged between the systems corresponding to the near and far field earthquakes. It is observed that period shifting due to SSI is larger for the first mode, the softer soil and the taller buildings and reaches up to 20 %. It decreases sharply as the mode number increases and is negligible for the higher modes. Also, difference of the corresponding periods of the same system but calculated by classical and nonclassical procedures is negligible.

Table 8 shows the damping ratios of the first three modes calculated for the nonclassical flexible-base Model 4 using Eq. (33).

It is interesting to compare the damping ratios collected in Tables 7 and 8. Values of the code-based damping ratios of Table 7 are essentially for the first mode. They begin from about 10 and 9 % for the 1-story building on the soil types D and E, respectively, and uniformly increase to about 14 % for the 20-story building. On the other hand, the first-mode damping ratios calculated using the equations of non-classical dynamical systems and reported in Table 8, vary from about 10 and 11–6 % for the same cases. There are two important differences here. First, the trend of variation of the damping ratio proves to be descending with the rigorous procedure in contrast to the one predicted by the code. Second, the rigorous damping ratio shows an asymptotic behavior such that from about the 10-story building, it does not change notably. Variation of the code-based ratio is not

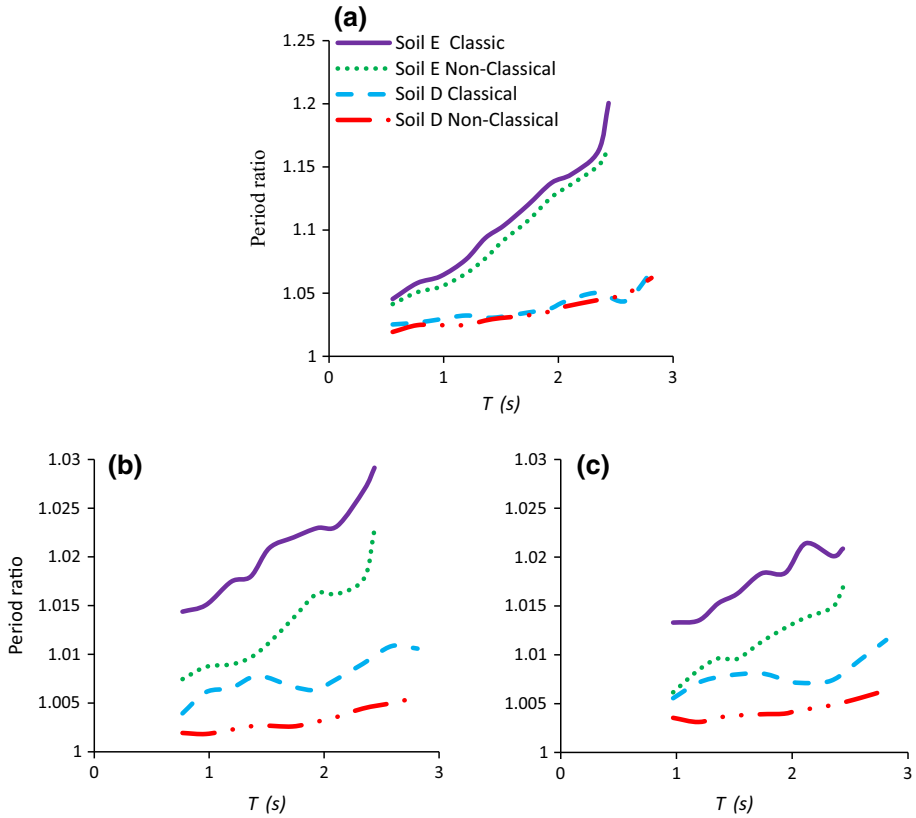


Fig. 6 Periods of the flexible-base models normalized to those of the fixed-base systems, versus the fixed-base period T . **a** First mode. **b** Second mode. **c** Third mode

Table 8 Damping ratios of the first three modes of the nonclassical SSI systems

Soil type	Type D			Type E		
	Mode 1 (%)	Mode 2 (%)	Mode 3 (%)	Mode 1 (%)	Mode 2 (%)	Mode 3 (%)
1	9.5	–	–	10.6	–	–
2	9	11.2	–	10.1	12.6	–
4	7.8	9.8	12.1	8.5	11	14.7
6	7.1	9.3	11.2	7.5	10.2	13.1
8	6.6	8.8	10.7	7	9.4	11.7
10	6.6	8.6	10.6	6.6	8.9	11
12	6.2	8.5	10.5	6.5	8.9	11.3
14	6.0	8.2	10.4	6.3	8.7	11
16	6.1	8.2	10.5	6.2	8.5	10.8
18	6	8.3	10.5	6	8.3	10.5
20	6	8.2	10.4	6.2	8.5	10.8

similar. Although values of damping ratios of the higher modes are larger than those of the first mode, as of Table 8, they show the same trend of variation.

5.3 Responses in the fundamental mode

A modal time history analysis is accomplished in the section. Only response of the first mode is included. Model 1 (see Sect. 4.3) is used for the fixed-base analysis and Models 3 and 4 for the flexible-base classical and nonclassical analysis, respectively. All of the response parameters are shown versus the fixed-base period of each building. Figure 7 shows the averaged maximum lateral displacement of roof normalized to the height of each building. In nonclassical analysis, it is calculated using Eq. (4). The results are presented for each soil type and each earthquake category.

According to Fig. 7, from a period of about 1 s, lateral displacements of the flexible-base models overtake those of the fixed-base model considerably, for both categories of earthquakes. The relative difference of displacements between models increases with height such that for the soil types D and E it reaches to about 33 and 56 %, respectively, for larger periods. For periods larger than 1 s, difference between the classical and nonclassical approaches for estimating the displacement response can be ignored. It should be noted that in the dynamic analysis of Model 3 the damping matrix is assumed to be

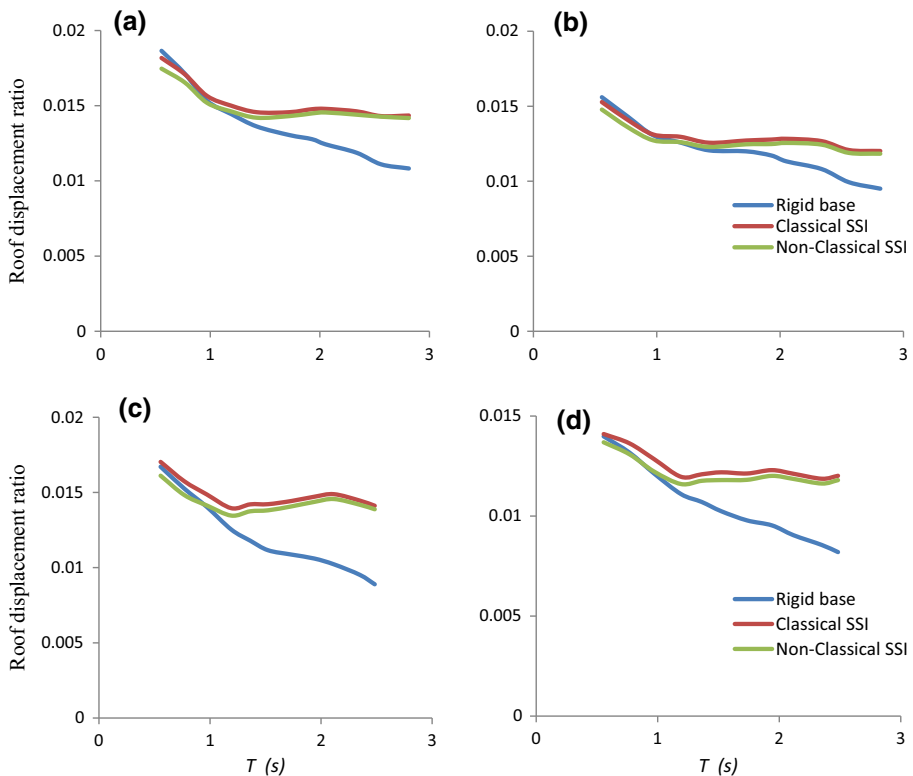


Fig. 7 The averaged maximum lateral displacement of roof normalized to the height of each building. **a** Soil type D, near field earthquakes. **b** Soil type D, far field earthquakes. **c** Soil type E, near field earthquakes. **d** Soil type E, far field earthquakes

proportional to the mass and stiffness matrices and only an equivalent modal damping ratio of 5 % is utilized. On the other hand, in the dynamic analysis of Model 4 that is nonclassical, the damping matrix is explicitly used and the modal damping ratios are calculated to be as reported in Table 8. According to this table, the nonclassical damping ratios of the first mode are about 6 % on both soil types for the periods above 1 s. Therefore, the maximum nonclassically calculated displacements should be slightly smaller than their classical counterparts in this period range, as they are.

For periods smaller than 1 s, difference between the displacements calculated by all of the three models is small and effect of SSI on displacements is negligible. It is interesting that in the same period range, the nonclassical analysis results in displacements smaller than those of the fixed-base and classical flexible-base models. Referring to Table 8, it seems that the damping augmented due to SSI in the nonclassical model is responsible for the smaller displacements in the shorter models. On the other hand, an increased contribution of the rocking motion in taller models overcomes the increased damping effect and results in larger displacements due to SSI. There is no conflict between the classical and nonclassical analysis in the latter case. As Fig. 2 shows, amplification of the structural response due to the soil properties occurs up to a maximum period of 1 s for the softer soil. Therefore larger SSI displacements of Fig. 7 after the 1 s period cannot be attributed to resonance.

The averaged maximum base shear of each system normalized to its weight is shown in Fig. 8. For the nonclassical analysis, it is calculated using Eq. (6).

Figure 8 shows that SSI decreases the base shear on both soil types. The reduction is important from the same 1 s period mentioned in displacement analysis. The more rigorous nonclassical analysis procedure is similar in results to the fixed-base case for periods smaller than 1 s and to the classical procedure for larger periods. The base shear reduction is up to 23 and 38 % for taller buildings.

Comparing Figs. 7 and 8, an important fact emerges. For periods smaller than 1 s, soil-structure interaction may not be taken into account for seismic analysis of structures similar to the ones of this study, i.e., moment frame structures resting on surface foundations. This is because use of the more accurate nonclassical SSI analysis results in response values similar to the fixed-base ones. Therefore, accounting for SSI with classical analysis underestimates the responses in this period range.

Figure 8 actually displays the first-mode spectral accelerations (normalized to g) of the studied buildings because in this figure the base shear is normalized to the building weight. The sample building code ASCE7-10 (American Society of Civil Engineers 2010) in its chapter on soil-structure interaction requires that the spectral acceleration including SSI is calculated using the fixed-base design spectrum but with flexible-base period of the first mode. The resulting value must be modified using the equivalent damping ratio of structure including SSI. Then the modified base shear due to SSI is calculated using Eq. (22):

$$\bar{V} = V - \Delta V \quad (22)$$

in which V and \bar{V} are the base shears without and with considering SSI, respectively, and ΔV is portion of the base shear deducted when accounting for SSI. ΔV is calculated using Eq. (23):

$$\Delta V = \left[C_s - \bar{C}_s \left(\frac{0.05}{\beta} \right)^{0.4} \right] \bar{W} \leq 0.3V \quad (23)$$

where C_s and \bar{C}_s are the seismic coefficients determined using the fundamental periods of the fixed-base and flexible-base systems, respectively, and β is damping ratio of the SSI

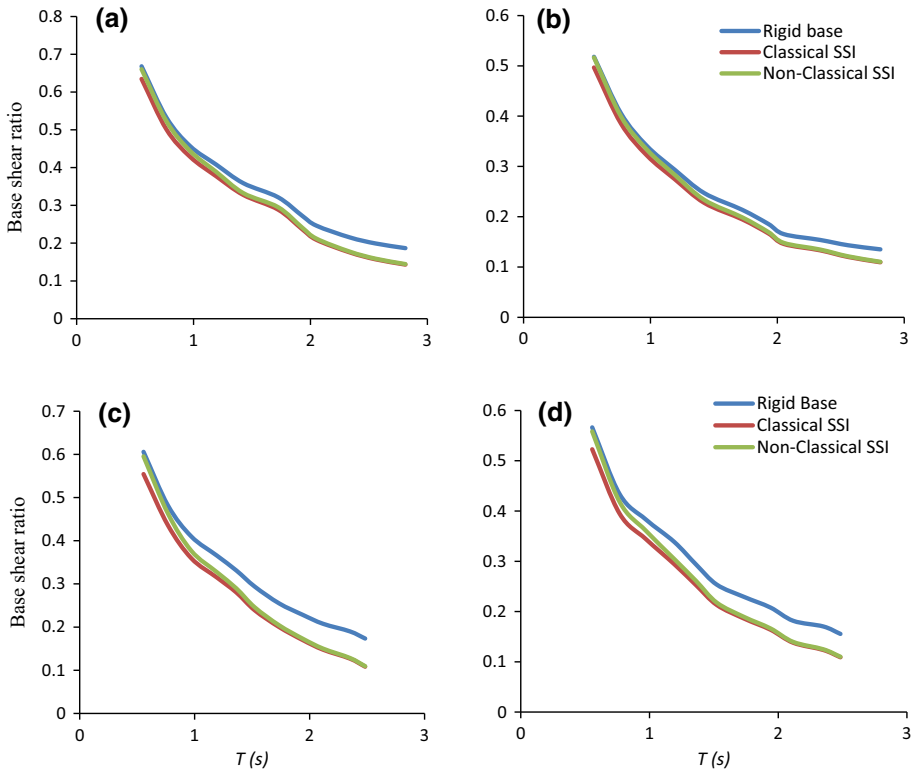


Fig. 8 Averaged maximum base shear normalized to the building weight. **a** Soil type D, near field earthquakes. **b** Soil type D, far field earthquakes. **c** Soil type E, near field earthquakes. **d** Soil type E, far field earthquakes

system calculated using Eq. (19). With the damping ratios calculated in Sect. 4.3.2 (see Table 7) and the natural periods mentioned in Sect. 5.2, it is now possible to construct a code-based first-mode spectrum including SSI using the fixed-base spectrum of Fig. 8. For this purpose, the spectral ordinate at the fundamental SSI period of each building is taken from the fixed-base spectrum of Fig. 8 and is corrected using the damping ratio of the SSI system (Table 7) by the correction factor of Sect. 4.3.2. The resulting values are depicted against the fixed-base fundamental period of each building and called the SSI-code spectrum. It is illustrated in Fig. 9 after being normalized to the fixed-base responses of the code. The nonclassical spectra of the flexible-base buildings, extracted from Fig. 8 after normalizing to the fixed-base responses in the same figure, are also illustrated for comparison. For the ease of reference, the latter values are averaged between the near and far field earthquakes.

Figure 9 reveals the important fact that how the code-based formula (Eqs. 22 and 23) underestimate the seismic response of an SSI system. While the spectral acceleration ratio using the rigorous method varies between 1 and 0.83 for the soil type D and between 1 and 0.71 for the soil type E as the period increases to about 3 s, similar code-based ratios are between 0.88 and 0.75, and, 0.86 and 0.73, respectively.

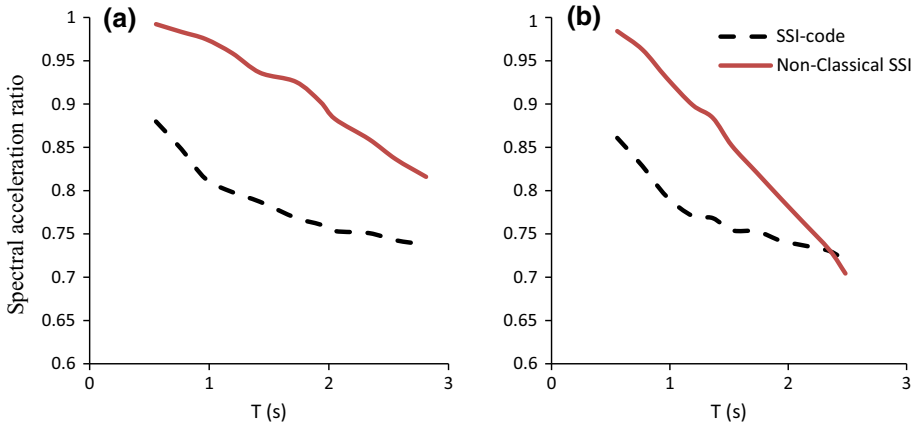


Fig. 9 The SSI-code and the flexible base nonclassical spectra averaged between near and far field earthquakes, both normalized to the corresponding rigid-base spectra. **a** Soil type D. **b** Soil type E

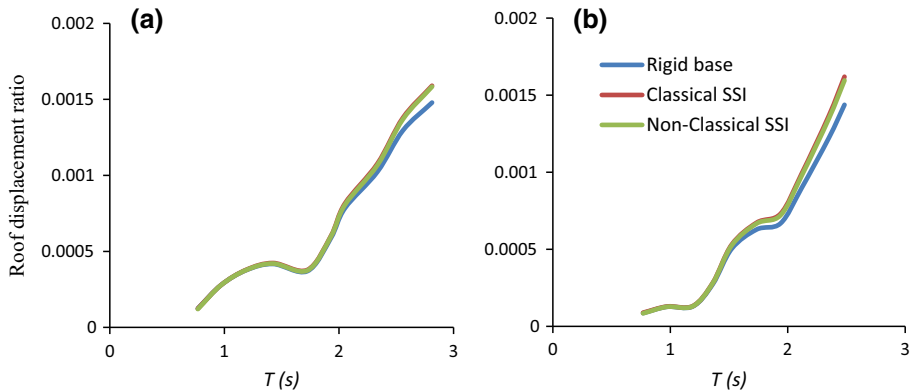


Fig. 10 The averaged maximum roof displacement corresponding to the higher modes, normalized to the building height. **a** Soil type D. **b** Soil type E

5.4 Responses in the higher modes

In Sect. 5.3 only the part of the total response corresponding to the first mode was presented. In the current section sum of the response corresponding to all other modes (called the higher modes) is illustrated. The averaged maximum values of roof displacement and base shear normalized to the building height and building weight, are shown in Figs. 10 and 11, respectively, for the three analysis cases. The values have been also averaged between near and far field earthquakes.

Based on Figs. 10 and 11, it can be said that response in the higher modes can equally be calculated using classical or nonclassical analysis. Therefore, use of nonclassical analysis is not necessary for the higher modes. On the other hand, for the building-soil systems studied and alike, accounting for SSI in the higher modes is important for systems with fixed-base fundamental periods larger than 2.5 s when calculating displacements and

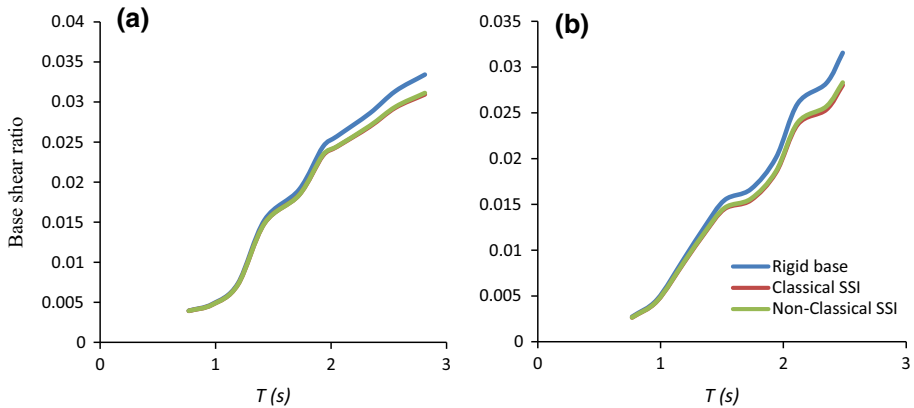


Fig. 11 The averaged maximum base shear corresponding to the higher modes, normalized to the building weight. **a** Soil type D. **b** Soil type E

larger than 2 s when deriving the base shear. In such ranges, higher mode displacements increase and base shears decrease considerably due to SSI.

5.5 Nonclassical spectral analysis

The nonclassical procedure of spectral analysis developed in Sect. 3 is used in this section to calculate the maximum roof displacement and base shear, using Eq. (12), in comparison with the results of the nonclassical time history analysis, using Eqs. (4) and (6), presented in Sects. 5.3 and 5.4. For spectral analysis, average of the response spectra of the earthquakes associated with each building (Table 4) are used. The spectral ordinates are corrected using the reduction factor introduced in Eq. (20). The CQC rule is used to combine the spectral responses of different modes. Therefore, the nonclassical spectral analysis of this study is approximate with respect to the nonclassical time history analysis, in several aspects: (1) Use of the SRSS rule to combine the maxima of the two terms on the right sides of Eqs. (4) and (6) to calculate the maximum responses presented in Eq. (8); (2) Use of the CQC rule to combine the maximum responses of different modes; (3) Use of an approximate relation between the pseudo-velocity and the relative velocity of the j th mode (Eq. 9); (4) Use of an approximate equation for correcting the spectral values due to a modified damping with SSI (Eq. 20). The response results of this section show the effects of above approximations.

The maximum roof displacement and base shear are illustrated in Figs. 12 and 13, respectively.

The maximum relative differences of associated time-history and spectral responses in Figs. 12 and 13 are 12 and 8 % for displacement and base shear, respectively. Therefore, the assumptions made to develop the equations of the nonclassical spectral analysis are justified within the SSI systems studied.

5.6 Correction factors for internal forces and lateral displacements due to SSI

Results of the averaged maximum displacements and base shears of the studied structures presented in Sect. 5.3 suggest that the frame structures can be analyzed as usual on a fixed

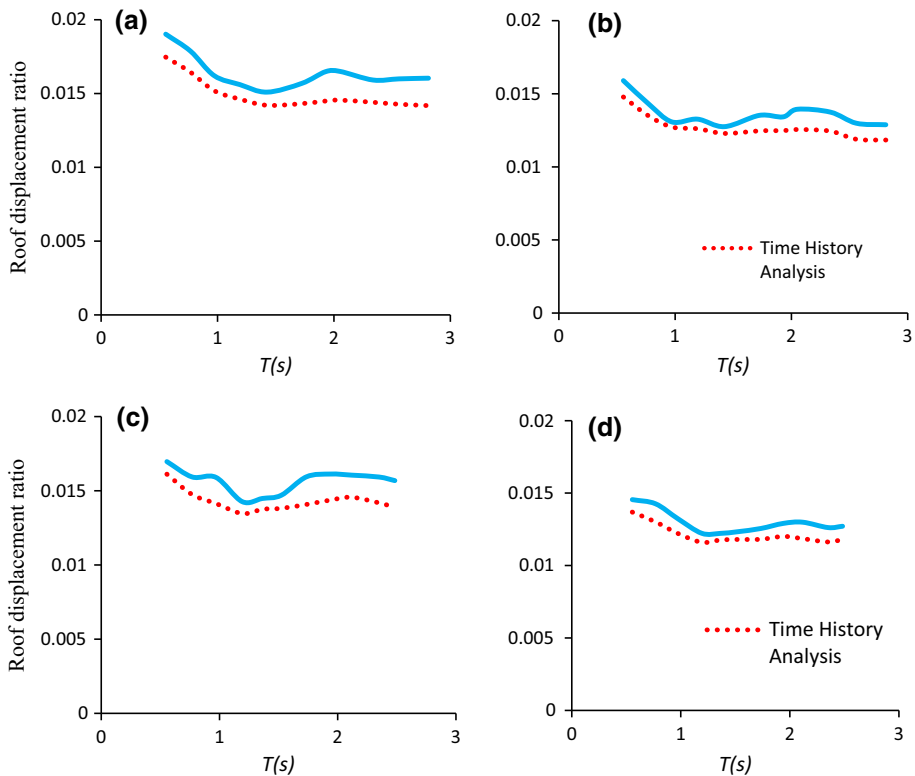


Fig. 12 Averaged maximum roof displacement normalized to the building height, using nonclassical time history and spectral analysis. **a** Soil type D, near field earthquakes. **b** Soil type D, far field earthquakes. **c** Soil type E, near field earthquakes. **d** Soil type E, far field earthquakes

base and then their lateral displacements and base shears can be increased and decreased, respectively, due to SSI using simple correction factors. Since the spectra of Sect. 5.3 have been plotted using the fixed-base fundamental period of the buildings, the effect of period lengthening has been already included and the correction factors only contain the effect of augmented damping where applicable. On the other hand, the factors are functions of the fixed-base fundamental period of a moment frame structure resting on surface foundations on the soil types D and E. Sections 5.3 and 5.4 present the fundamental and higher mode responses, respectively. Similarly, the total responses could be shown. Then, the correction factors have been calculated both for the fundamental mode responses and the total responses including all modes. According to Sect. 5.4, for the buildings of the type investigated in this study, difference between the two groups of correction factors is considerable only from a period of about 2 s upward. The correction factors are calculated by curve fitting of the fixed-base results of Sect. 5.3 to the more accurate nonclassical responses of the same section in order to have a best fit.

Tables 9 and 10 illustrate equations of the correction factors. They have been determined by averaging between the results of the near and far-field earthquakes and are only necessary to be used for the period range of $T \geq 1$ s. Out of the mentioned range SSI has minimal effects for the cases studied and may not be taken into account, based on Sect. 5.3. The correction factors can be equally applied to the design spectrum or to the results of

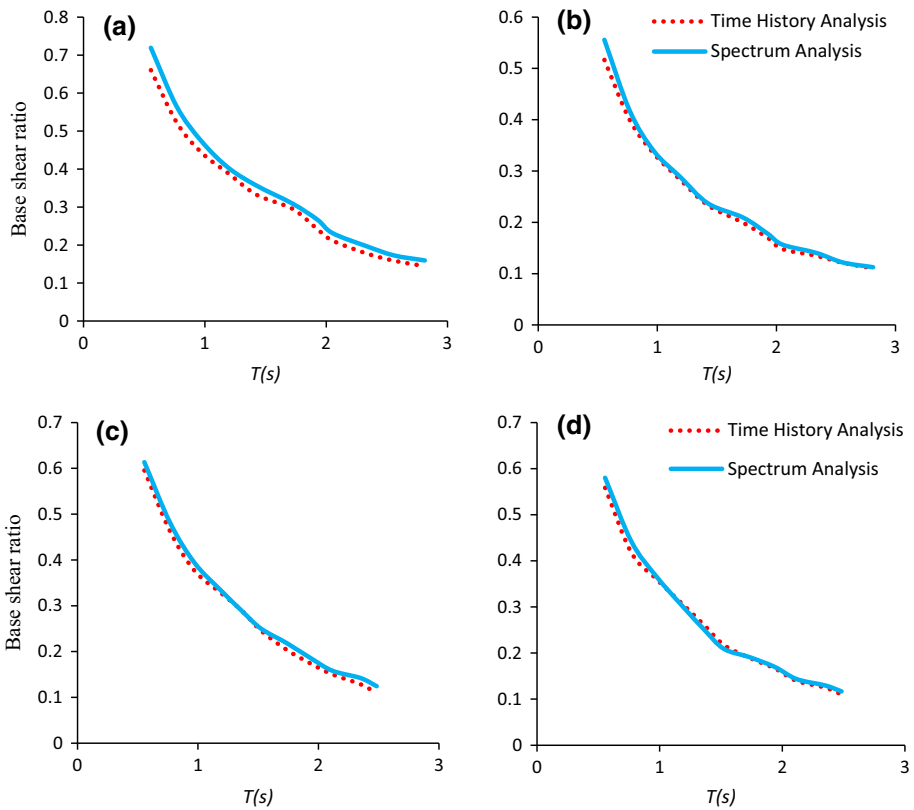


Fig. 13 Averaged maximum base shear normalized to the building weight using nonclassical time history and spectral analysis. **a** Soil type D, near field earthquakes. **b** Soil type D, far field earthquakes. **c** Soil type E, near field earthquakes. **d** Soil type E, far field earthquakes

Table 9 Correction factors for the base shear or internal forces, α_V

Soil type D		
Total response		$\alpha_V = -0.088T + 1.069$
First mode response		$\alpha_V = -0.103T + 1.091$
Soil type E		
Total response		$\alpha_V = -0.147T + 1.076$
First mode response		$\alpha_V = -0.168T + 1.100$

Table 10 Correction factors for the lateral displacements and rotations, α_U

Soil type D		
Total response		$\alpha_U = +0.164T + 0.782$
First mode response		$\alpha_U = +0.185T + 0.747$
Soil type E		
Total response		$\alpha_U = +0.277T + 0.735$
First mode response		$\alpha_U = +0.313T + 0.689$

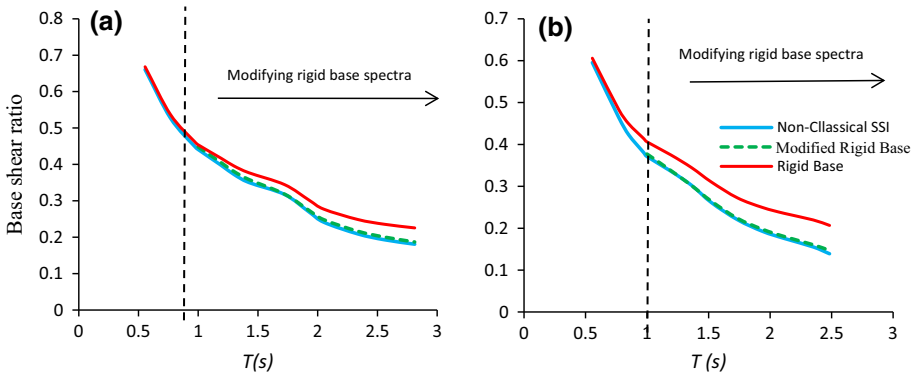


Fig. 14 Correction of fixed-base base shear (normalized to the building weight) due to SSI. **a** Soil type D. **b** Soil type E

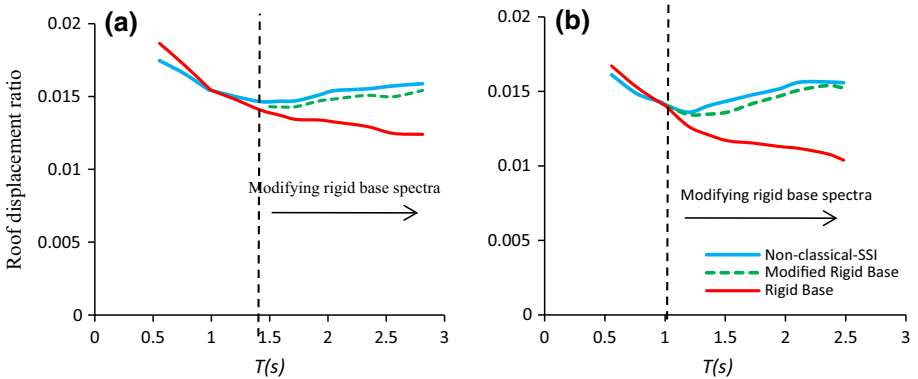


Fig. 15 Correction of the lateral roof displacement (normalized to the building height) due to SSI. **a** Soil type D. **b** Soil type E

spectral analysis including internal forces and deformations of fixed-base moment frame structures, as follows:

$$\text{SSI response} = \text{fixed-base response} \times \text{correction factor.}$$

Figures 14 and 15 show the results of correction of the fixed-base total responses, using Tables 9 and 10, in comparison to the nonclassical SSI results of Sect. 5.3. The figures describe the accuracy of the correction process.

6 Conclusions

In this study the theory of the modal analysis of nonclassical systems was illustrated for systems resting on flexible bases, representative of soil-structure interaction problems. Several structures having one to twenty stories resting on two types of soils, being medium and soft, were analyzed each one under two suits of ten consistent and scaled earthquake

motions specific to that structure recorded at near and far distances. Modal time history and spectrum analysis were accomplished in their classical and non-classical versions.

The important results of the study, for the buildings and the soils considered, can be summarized as follows:

1. Period shifting due to SSI is larger for the fundamental mode, the softer soil and the taller buildings and reaches up to 20 %. It decreases gradually as the mode number increases. Periods of flexible-base systems can be almost equally calculated by classical and nonclassical procedures.
2. The first-mode code-based damping ratios begin from about 10 and 9 % for the 1-story building on the soil types D and E, respectively, and uniformly increase to about 14 % for the 20-story building. On the other hand, the first-mode damping ratios calculated using the equations of non-classical dynamical systems, vary from about 10 and 11–6 % for the same cases. Therefore, variation of the damping ratio is descending with the rigorous procedure and ascending according to the code. Also, dissimilar to the code, the rigorous damping ratio shows an asymptotic behavior such that from about the 10-story building, it does not change notably. Values of damping ratios of the higher modes are larger than those of the first mode, and show a trend of variation similar to the first mode.
3. The relative difference of displacements between the associated fixed-base and flexible-base models becomes important from a period of about 1 s and increases with height, and is larger for the softer soil. For periods smaller than 1 s, the nonclassical analysis results in displacements somewhat smaller than those of the fixed-base model.
4. SSI decreases the base shear on both soil types. The reduction is important again from a period of 1 s. Results of SSI analysis with the nonclassical procedure are similar to the fixed-base case for periods smaller than 1 s and to the classical SSI procedure for larger periods. The base shear reduction is up to 23 and 38 % for taller buildings on the soil types D and E, respectively.
5. For periods smaller than 1 s, soil-structure interaction may not be taken into account for seismic analysis of moment frame structures resting on surface foundations.
6. The code-prescribed process of inclusion of SSI underestimates the base shear in the whole period range studied. Underestimation is more critical for the soil type D.
7. Use of nonclassical SSI analysis is not necessary for the higher modes. Accounting for SSI in the higher modes is important for systems with fixed-base fundamental periods larger than 2.5 s when calculating (increased) displacements and larger than 2 s when deriving the (decreased) base shear.
8. The simplifying assumptions for the nonclassical SSI spectral analysis are justified for the SSI systems studied.
9. Maxima of the lateral displacements and base shear can be calculated using conventional spectral analysis of fixed-base structures and converted to the responses including SSI using the simple correction factors presented in this study.

Finally, it should be noted that the mentioned conclusions are only applicable to the cases studied, namely, buildings consisting of moment frames resting on surface foundations. Regarding the soil medium, a uniform halfspace with characteristics representative of soft soils was considered. For the exceptional case of a soft surface layer resting on a very stiff soil the radiation damping of the oscillating structure might diminish. The above limitations should be taken into account when using the results of this study.

Appendix 1: Equations of motion

The equations of motion of the system of Fig. 1 can be written as follows:

$$[M] \begin{Bmatrix} \{\ddot{u}\} \\ \ddot{u}_b \\ \ddot{\psi} \end{Bmatrix} + [C] \begin{Bmatrix} \{\dot{u}\} \\ \dot{u}_b \\ \dot{\psi} \end{Bmatrix} + [K] \begin{Bmatrix} \{u\} \\ u_b \\ \psi \end{Bmatrix} = - \begin{Bmatrix} \{m\} \\ m_b + \sum_1^n m_i \\ \sum_1^n m_i h_i \end{Bmatrix} \ddot{u}_g(t) = \{p(t)\} \quad (24)$$

in which:

$$[M] = \begin{bmatrix} [m] & \{m\} & \{mh\} \\ \{m\}^T & m_b + \sum_1^n m_i & \sum_1^n m_i h_i \\ \{mh\}^T & \sum_1^n m_i h_i & I + \sum_1^n m_i h_i^2 \end{bmatrix} \quad (25)$$

$$[C] = \begin{bmatrix} [c] & \{0\} & \{0\} \\ \{0\}^T & c_{uu} & 0 \\ \{0\}^T & 0 & c_{\psi\psi} \end{bmatrix}$$

$$[K] = \begin{bmatrix} [k] & \{0\} & \{0\} \\ \{0\}^T & k_{uu} & 0 \\ \{0\}^T & 0 & k_{\psi\psi} \end{bmatrix}$$

and:

$$[m] = \begin{bmatrix} m_1 & & & & & \\ & m_2 & 0 & & & \\ & & \ddots & & & \\ & & & m_{n-1} & & \\ & 0 & & & m_n & \end{bmatrix}$$

$$[c] = \begin{bmatrix} c_1 & -c_2 & \cdots & 0 & 0 \\ -c_2 & c_1 + c_2 & -c_3 & 0 & 0 \\ \vdots & \vdots & \ddots & \vdots & \vdots \\ 0 & 0 & \cdots & c_{n-1} + c_{n-2} & -c_n \\ 0 & 0 & \cdots & -c_n & c_n + c_{n-1} \end{bmatrix} \quad (26)$$

$$[K] = \begin{bmatrix} k_1 + k_2 & -k_2 & \cdots & 0 & 0 \\ -k_2 & k_2 + k_3 & -k_3 & 0 & 0 \\ \vdots & -k_3 & \ddots & \vdots & \vdots \\ 0 & \vdots & \cdots & k_n + k_{n+1} & -k_{n-1} \\ 0 & 0 & \cdots & -k_{n-1} & k_n \end{bmatrix}$$

and:

$$\begin{aligned} \{m\} &= [m_1 \quad m_2 \quad \dots \quad m_n]^T \\ \{mh\} &= [m_1h_1 \quad m_2h_2 \quad \dots \quad m_nh_n]^T \\ \{u\} &= [u_1 \quad u_2 \quad \dots \quad u_n]^T \\ I &= I_b + \sum_{i=1}^n I_i \end{aligned} \tag{27}$$

In the above equations, m_i and m_b ($i = 1, 2, \dots, n; n =$ number of stories) are mass of the i th floor and the foundation, respectively, h_i is the height of the i th floor from the base, I_i and I_b are respectively the mass moments of inertia of the i th story and the foundation, c_i and k_i are the damping coefficient and the lateral relative stiffness of the i th story, respectively, c_{jj} and k_{jj} with $j = u$ or ψ are respectively the damping and stiffness impedances of the supporting medium in translational and rotational directions, u_i, u_b and u_g are the horizontal displacements of the i th story, the foundation, and ground with respect to a fixed reference, respectively, ψ is the rotational component of motion of foundation, and a dot represents derivation with respect to time.

Appendix 2: The free vibration response characteristics

The homogeneous solution of Eq. (24) can be written as:

$$\{U\} = \{\psi\}e^{rt} \tag{28}$$

in which r and $\{\psi\}$ are the characteristic value and vector, respectively, and $\{U\}$ is defined in Eq. (2). Substitution of (28) in (24) with $p(t) = 0$ gives:

$$(r^2[M] + r[C] + [K])\{\psi\} = \{0\} \tag{29}$$

Foss (1958) showed that the characteristic Eq. (29) can be reduced to:

$$(r[A] + [B])\{Z\} = \{0\} \tag{30}$$

in which:

$$\{Z\} = \left\{ \begin{matrix} r\{\psi\} \\ \{\psi\} \end{matrix} \right\} \tag{31}$$

$$[A] = \begin{bmatrix} [0] & [M] \\ [M] & [C] \end{bmatrix}_{2N \times 2N}$$

$$[B] = \begin{bmatrix} -[M] & [0] \\ [0] & [K] \end{bmatrix}_{2N \times 2N}$$

The dimension of Eq. (30) is $2N$ where $N = n + 2$ with the additional two DOF's of the foundation included. Its solution results in N complex conjugates for r and ψ . If r_j and

\bar{r}_j are a pair of characteristic values and $\{\psi\}$ and $\{\bar{\psi}\}$ a pair of characteristic vectors where the over bar denotes complex conjugate, then the following relations are introduced:

$$\left. \begin{matrix} r_j \\ \bar{r}_j \end{matrix} \right\} = -q_j \pm \tilde{p}_j \tag{32}$$

$$\left. \begin{matrix} \{\psi_j\} \\ \{\bar{\psi}_j\} \end{matrix} \right\} = \{\phi_j\} \pm i\{\chi_j\}$$

in which $i = \sqrt{-1}$, q_j and \tilde{p}_j are real constants, and, $\{\phi_j\}$ and $\{\chi_j\}$ are N-component real vectors. Then the new parameters p_j and ξ_j are defined as follows:

$$p_j = \sqrt{q_j^2 + \tilde{p}_j^2} \tag{33}$$

$$\xi_j = \frac{q_j}{p_j}$$

Then:

$$\left. \begin{matrix} r_j \\ \bar{r}_j \end{matrix} \right\} = -\xi_j p_j \pm i\tilde{p}_j \tag{34}$$

$$\tilde{p}_j = p_j \sqrt{1 - \xi_j^2}$$

Substituting Eq. (32) in (28) results in:

$$\{U_j\} = e^{-\xi_j p_j t} (\{\phi_j\} \pm i\{\chi_j\}) e^{\pm \tilde{p}_j t} \tag{35}$$

The displacement response in Eq. (35) consists of two parts: the damped amplitude and the oscillation function, which are as follows:

$$\text{Displacement amplitude} = e^{-\xi_j p_j t} (\{\phi_j\} \pm i\{\chi_j\}) \tag{36}$$

$$\text{Oscillation function} = e^{\pm \tilde{p}_j t} = \cos(\tilde{p}_j t) \pm i \sin(\tilde{p}_j t) \tag{37}$$

Equation (36) shows that ξ_j is the damping ratio of the jth mode while p_j and \tilde{p}_j show the undamped and damped frequencies of the jth mode, respectively, all being positive values.

The total response in the jth mode ($j = 1, 2, \dots, N$) can be calculated combining contributions from both complex conjugates as:

$$\{U_j\} = C_j \{\psi_j\} e^{r_j t} + \bar{C}_j \{\bar{\psi}_j\} e^{\bar{r}_j t} \tag{38}$$

in which C_j is a complex constant. Equation (38) can be simplified as:

$$\{U_j\} = 2Re[C_j \{\psi_j\} e^{r_j t}] \tag{39}$$

in which Re denotes real value. Summing the combinations of all modes, the total response at each degree of freedom can be written as:

$$\{U\} = 2 \sum_{j=1}^N Re \left[C_j \{\psi_j\} e^{r_j t} \right] \tag{40}$$

Using modal orthogonality conditions, it can be shown that (Veletsos and Ventura 1986):

$$C_j = \frac{r_j \{\psi_j\}^T [M] \{U(0)\} + \{\psi_j\}^T [C] \{U(0)\} + \{\psi_j\}^T [M] \{\dot{U}(0)\}}{2r_j \{\psi_j\}^T [M] \{\psi_j\} + \{\psi_j\}^T [C] \{\psi_j\}} \tag{41}$$

in which $\{U(0)\}$ and $\{\dot{U}(0)\}$ are the vectors of initial displacement and initial velocity of the system.

Appendix 3: The displacement response to base acceleration

Response of the system of Fig. (1) to a base acceleration that is equivalent to a constant initial velocity at all horizontal degrees of freedom, can be calculated from Eqs. (40) and (41) with the following initial values:

$$\{U(0)\} = \{0\}, \{\dot{U}(0)\} = \begin{Bmatrix} 1 \\ \vdots \\ 1 \\ 1 \\ 0 \end{Bmatrix} v_0 \tag{42}$$

in which v_0 is the value of the initial velocity. Substituting Eq. (42) in (41) results in:

$$B_j = \frac{\{\psi_j\}^T [M] \langle 1 \quad \dots \quad 1 \quad 1 \quad 0 \rangle_{n+2}^T}{2r_j \{\psi_j\}^T [M] \{\psi_j\} + \{\psi_j\}^T [C] \{\psi_j\}} \tag{43}$$

in which $B_j = C_j/v_0$. Now, Eq. (43) is substituted in (40) to result in:

$$\{U\} = 2 \sum_{j=1}^N Re [B_j \{\psi_j\} v_0 e^{r_j t}]. \tag{44}$$

To write the response in the real form, the amplitude in (44) is decomposed as follows:

$$2B_j \{\psi_j\} = \left\{ \beta_j^v \right\} + i \left\{ \gamma_j^v \right\} \tag{45}$$

in which $\left\{ \beta_j^v \right\}$ and $\left\{ \gamma_j^v \right\}$ are real and imaginary parts of the term on the left. Substituting (45) in (44) gives:

$$\{U\} = \sum_{j=1}^N e^{-\xi_j p_j t} \left[\left\{ \beta_j^v \right\} \cos(\tilde{p}_j t) - \left\{ \gamma_j^v \right\} \sin(\tilde{p}_j t) \right] v_0 \tag{46}$$

The unit impulse response function for the system is introduced as:

$$h_j(t) = \frac{1}{\tilde{p}_j} e^{-\xi_j p_j t} \sin(\tilde{p}_j t) \tag{47}$$

The derivative of Eq. (47) is:

$$\dot{h}_j(t) = e^{-\xi_j p_j t} \left[\cos(\tilde{p}_j t) - \frac{\xi_j}{\sqrt{1 - \xi_j^2}} \sin(\tilde{p}_j t) \right] \tag{48}$$

Replacing (47) and (48) in (46) results in:

$$\{U\} = \sum_{j=1}^N \left[\{\alpha_j^v\} p_j h_j(t) - \{\beta_j^v\} \dot{h}_j(t) \right] v_0 \tag{49}$$

in which:

$$\{\alpha_j^v\} = \xi_j \{\beta_j^v\} - \sqrt{1 - \xi_j^2} \{\gamma_j^v\} \tag{50}$$

For calculating the response at $t_0 = \tau$ to a base acceleration $\ddot{u}_g(t)$, the velocity $v(\tau)$ is computed as:

$$v(t) = -\dot{u}_g(\tau) dt \tag{51}$$

If Eq. (51) is substituted in (49) and integrated to the arbitrary time t , the dynamic response will be resulted as Eq. (4).

Appendix 4: The base shear

To calculate the base shear due to ground motion, first the vector of lateral story forces is computed using (24) as:

$$\{f\} = [M]\{\ddot{U}\}^{total} = -([K]\{U\} + [C]\{\dot{U}\}) \tag{52}$$

$\{\dot{U}\}$ and $\{U\}$ are determined from (44) and replaced in (52) to give:

$$\{f(t)\} = 2 \sum_{j=1}^N Re \left\{ [K]\{\psi_j\} + r_j [C]\{\psi_j\} \right\} B_j v_0 e^{r_j t} \tag{53}$$

Using the homogenous form of (24) with (28) in (53), $f(t)$ is written as:

$$\{f(t)\} = -2 \sum_{j=1}^N Re \left\{ r_j^2 [M]\{\psi_j\} \right\} B_j v_0 e^{r_j t} \tag{54}$$

Using Eqs. (45), (47), and (48) in (54) and integrating, give the vector of lateral forces as follows:

$$\{f(t)\} = \sum_{j=1}^N e^{-\xi_j p_j t} [M] \left\{ \left[(p_j^2 - 2\xi_j^2 p_j^2) \left(\{\beta_j^v\} \cos(\bar{p}_j t) - \{\gamma_j^v\} \sin(\bar{p}_j t) \right) \right] + \left[\left(-2i\xi_j p_j^2 \sqrt{1 - \xi_j^2} \right) \left(\{\beta_j^v\} \sin(\bar{p}_j t) + \{\gamma_j^v\} \cos(\bar{p}_j t) \right) \right] \right\} v_0 \tag{55}$$

in which:

$$\{\omega_j^v\} = \xi_j \{\gamma_j^v\} + \sqrt{1 - \xi_j^2} \{\beta_j^v\} \tag{56}$$

Equation (55) can also be written as:

$$\{f(t)\} = \sum_{j=1}^N \{\alpha_j^{Mv}\} p_j V_j(t) + \sum_{j=1}^N \{\beta_j^{Mv}\} \dot{D}_j(t) + \sum_{j=1}^N \{\omega_j^{Mv}\} p_j V_j(t) + \sum_{j=1}^N \{\gamma_j^{Mv}\} \dot{D}_j(t) \tag{57}$$

where:

$$\begin{aligned} \{\alpha_j^{Mv}\} &= (p_j + 2\xi_j^2 p_j) [M] \{\alpha_j^v\} \\ \{\beta_j^{Mv}\} &= (p_j + 2\xi_j^2 p_j) [M] \{\beta_j^v\} \\ \{\omega_j^{Mv}\} &= \left(-2\xi_j p_j^2 \sqrt{1 - \xi_j^2} \right) \{\omega_j^v\} \\ \{\gamma_j^{Mv}\} &= \left(-2\xi_j p_j^2 \sqrt{1 - \xi_j^2} \right) \{\gamma_j^v\} \end{aligned} \tag{58}$$

Then the base shear is computed as the summation of lateral story forces resulting in Eq. (6).

Appendix 5: Characteristics of the selected records

The earthquake records selected with the criteria of this study are described in the following table.

Order	NGA no.	EQ. name	Date	Station	Soil type	Distance (km)	Max Acc. (g)
1	169	Imperial Valley-06	10/15/79	DELTA	D	22.0	0.28
2	178	Imperial Valley-06	10/15/79	El Centro Array #3	E	12.85	0.26
3	726	Superstition Hills-02	11/24/87	Salton Sea Wildlife Refuge	E	25.88	0.13
4	732	Loma Prieta	10/18/89	APEEL 2—Redwood City	E	43.23	0.08

Order	NGA no.	EQ. name	Date	Station	Soil type	Distance (km)	Max Acc. (g)
5	777	Loma Prieta	10/15/79	HOLLISTER CITY HALL	D	27.6	0.23
6	778	Loma Prieta	10/18/89	Hollister Differential Array	D	24.8	0.26
7	786	Loma Prieta	10/18/89	Palo Alto—1900 Embarc	D	30.81	0.21
8	806	Loma Prieta	10/18/89	Sunnyvale Colton Ave	D	24.23	0.21
9	953	Northridge-01	01/17/94	Beverly Hills—14145 Mulhol	D	17.15	0.55
10	987	Northridge-01	1/17/94	LA—Centinela St	D	28.3	0.25
11	995	Northridge-01	01/17/94	LA—Hollywood Stor FF	D	24.03	0.37
12	996	Northridge-01	01/17/94	LA—FARING RD	D	20.81	0.34
13	1001	Northridge-01	01/17/94	LA—S Grand Ave	D	33.99	0.27
14	1003	Northridge-01	01/17/94	LA—Saturn St	D	27.01	0.45
15	1038	Northridge-01	1/17/94	Montebello Bluff	E	45.03	0.15
16	1044	Northridge-01	01/17/94	Newhall—Fire Sta	D	5.92	0.70
17	1063	Northridge-01	1/17/94	Rinaldi Receiving Sta	D	6.5	0.63
18	1085	Northridge-01	01/17/94	SYLMAR-CONVERTER STA-EAST	D	5.19	0.65
19	1087	Northridge-01	01/17/94	Tarzana—Cedar Hill A	D	15.6	0.99
20	1107	Kobe, Japan	01/16/95	Kakogawa	D	22.5	0.35
21	1111	Kobe, Japan	01/16/95	Nishi—Akashi	E	7.08	0.49
22	1113	Kobe, Japan	01/16/95	Osaj	E	21.35	0.08
23	1116	Kobe, Japan	01/16/95	Shin—Osaka	E	19.15	0.23
24	1119	Kobe, Japan	01/16/95	Takarazu	E	0.27	0.71
25	1120	Kobe, Japan	01/16/95	Takatori	E	1.47	0.65
26	1180	Chi—Chi, Taiwan	09/20/99	CHY002	E	24.96	0.13
27	1183	Chi—Chi, Taiwan	09/20/99	CHY008	E	40.43	0.12
28	1186	Chi—Chi, Taiwan	09/20/99	CHY014	D	34.18	0.24

Order	NGA no.	EQ. name	Date	Station	Soil type	Distance (km)	Max Acc. (g)
29	1187	Chi–Chi, Taiwan	09/20/99	CHY015	D	38.13	0.16
30	1194	Chi–Chi, Taiwan	09/20/99	CHY025	E	19.07	0.15
31	1196	Chi–Chi, Taiwan	09/20/99	CHY027	E	41.99	0.06
32	1197	Chi–Chi, Taiwan	09/20/99	CHY028	D	3.12	0.79
33	1199	Chi–Chi, Taiwan	09/20/99	CHY032	E	35.43	0.09
34	1201	Chi–Chi, Taiwan	09/20/99	CHY034	D	14.82	0.30
35	1203	Chi–Chi, Taiwan	09/20/99	CHY036	D	16.04	0.26
36	1204	Chi–Chi, Taiwan	09/20/99	CHY039	E	31.87	0.11
37	1205	Chi–Chi, Taiwan	09/20/99	CHY041	E	19.83	0.46
38	1228	Chi–Chi, Taiwan	09/20/99	CHY076	E	42.15	0.08
39	1233	Chi–Chi, Taiwan	09/20/99	CHY082	E	36.09	0.07
40	1236	Chi–Chi, Taiwan	09/20/99	CHY088	D	37.48	0.18
41	1238	Chi–Chi, Taiwan	09/20/99	CHY092	E	22.69	0.10
42	1240	Chi–Chi, Taiwan	09/20/99	CHY094	E	37.1	0.06
43	1246	Chi–Chi, Taiwan	09/20/99	CHY104	E	18.02	0.18
44	1478	Chi–Chi, Taiwan	09/20/99	TCU033	D	40.88	0.18
45	1483	Chi–Chi, Taiwan	09/20/99	TCU040	E	22.06	0.13
46	1484	Chi–Chi, Taiwan	09/20/99	TCU042	D	26.31	0.21
47	1492	Chi–Chi, Taiwan	09/20/99	TCU052	D	0.66	0.35
48	1496	Chi–Chi, Taiwan	09/20/99	TCU056	E	10.48	0.14
49	1503	Chi–Chi, Taiwan	09/20/99	TCU065	D	0.57	0.66
50	1504	Chi–Chi, Taiwan	09/20/99	TCU067	D	0.62	0.41
51	1507	Chi–Chi, Taiwan	09/20/99	TCU071	D	5.8	0.62
52	1508	Chi–Chi, Taiwan	09/20/99	TCU072	D	7.08	0.40

Order	NGA no.	EQ. name	Date	Station	Soil type	Distance (km)	Max Acc. (g)
53	1509	Chi–Chi, Taiwan	09/20/99	TCU074	D	13.46	0.45
54	1529	Chi–Chi, Taiwan	09/20/99	TCU102	D	1.49	0.24
55	1536	Chi–Chi, Taiwan	09/20/99	TCU110	E	11.58	0.18
56	1537	Chi–Chi, Taiwan	09/20/99	TCU111	E	22.12	0.11
57	1538	Chi–Chi, Taiwan	09/20/99	TCU112	E	27.48	0.08
58	1541	Chi–Chi, Taiwan	09/20/99	TCU116	E	12.38	0.17
59	1542	Chi–Chi, Taiwan	09/20/99	TCU117	E	25.42	0.13
60	1553	Chi–Chi, Taiwan	09/20/99	TCU141	E	24.19	0.09
61	1602	DUZCE, Turkey	11/12/99	BOLU	D	12.04	0.77
62	1605	DUZCE, Turkey	11/12/99	DUZCE	D	6.58	0.43

References

- American Institute of Steel Construction (2005) Specification for structural steel buildings. AISC-ASD, Chicago
- American Society of Civil Engineers (2010) Minimum design loads for buildings and other structures, ASCE standard ASCE/SEI 7-10 including Supplement no. 1, American Society of Civil Engineers, Reston, Virginia
- American Society of Civil Engineers (2013) Seismic rehabilitation of existing buildings, ASCE/SEI 41-13. ASCE Publications, Reston
- Ashour SA (1987) Elastic seismic response of buildings with supplemental damping. Ph.D. Dissertation, Department of Civil Engineering, University of Michigan
- Bommer JJ, Mendis R (2005) Scaling of spectral displacement ordinates with damping ratios. *J Earthq Eng Struct Dyn* 34:145–165
- Computers and Structures, Inc. (2014) SAP2000, an integrated analysis and design software, version 17
- Eurocode No. 8 (2003) Design of structures for earthquake resistance, part 1: general rules, seismic actions and rules for buildings. CEN, Brussels
- Foss KA (1958) Coordinates which uncouple the equations of motion of damped linear dynamic system. *J Appl Mech ASME* 25:361–364
- Gazetas G (1991) Formulas and charts for impedances of surface and embedded foundations. *J Geotech Eng* 117:1363–1381
- Internet Site. http://peer.berkeley.edu/peer_ground_motion_database. Accessed May 2013
- Lin YY, Chang KC (2003) A Study on damping reduction factor for buildings under earthquake ground motions. *J Struct Eng* 129(2):206–214
- Newmark NM, Hall WJ (1982) Earthquake spectra and design. Engineering monographs on earthquake criteria, structural design, and strong motion records, earthquake engineering research institute, Berkeley, California
- Pekcan G, Mander JB, Chen SS (1999) Fundamental considerations for the design of non-linear viscous dampers. *J Earthq Eng Struct Dyn* 28:1405–1425

- Ramirez OM, Constantinou MC, Whittaker AS, Kircher CA, Chrysostomou CZ (2002) Elastic and inelastic seismic response of buildings with damping systems. *Earthq Spectra* 18(3):531–547
- Sadek F, Mohraz B, Riley MA (2000) Linear procedures for structures with velocity dependent dampers. *J Struct Eng* 126:887–895
- Sinha R, Igusa T (1995) CQC and SRSS methods for non-classically damped structures. *J Earthq Eng Struct Dyn* 24:615–619
- Song J, Chu Y, Liang Z, Lee GC (2008) Response-spectrum-based analysis for generally damped linear structures. In: *The 14 world conference on earthquake engineering, China, Beijing*
- Veletsos AS, Ventura CE (1986) Modal analysis of non-classical damped linear system. *Earthquake Eng Struct Dynam* 14:217–243
- Wu JP, Hanson RD (1989) Study of inelastic spectra with high damping. *J Struct Eng* 115:1412–1431
- Zhou XY, Yu RF (2008) Mode superposition method of non stationary seismic responses for non classically damped linear systems. *J Earthquake Eng* 12:473–516
- Ziaefar M, Tavousi S (2005) Mass participation in non-classical mass isolated systems. *Asian J Civ Eng (Build Hous)* 6:273–301